

Identification of Nonlinear and Near-field Effects in Jet Noise Using Nonlinearity Indicators

Kent L. Gee¹ and Micah R. Shepherd²

Department of Physics and Astronomy, Brigham Young University, Provo, UT, 84602

Lauren E. Falco³ and Anthony A. Atchley⁴

Graduate Program in Acoustics, The Pennsylvania State University, University Park, PA, 16802

Lawrence S. Ukeiley⁵

Mechanical and Aerospace Engineering Department, University of Florida, Shalimar, FL, 32579

Bernard J. Jansen⁶ and John M. Seiner⁷

National Center for Physical Acoustics, University of Mississippi, Oxford, MS, 38677

In the collection and analysis of high-amplitude jet noise data for nonlinear acoustic propagation, both model-scale and full-scale measurements have limitations. Model-scale measurements performed in anechoic facilities are usually limited by transducer and data acquisition system bandwidths and maximum propagation distance. The accuracy of full-scale measurements performed outdoors is reduced by ground reflections and atmospheric effects. This paper describes the use of two nonlinearity indicators as complementary to ordinary spectral analysis of jet noise propagation data. The first indicator is based on an ensemble-averaged version of the generalized Burgers equation. The second indicator is the bicoherence, which is a normalized version of the bispectral density. These indicators are applied to Mach-0.85 and Mach-2.0 unheated jet noise data collected at the National Center for Physical Acoustics. Specifically, the indicators are used to separate geometric near-field effects from nonlinear propagation effects for the Mach-2.0 data, which cannot be done conclusively using comparisons of power spectral densities alone.

Nomenclature

$\alpha(f)$	= atmospheric absorption coefficient
β	= coefficient of nonlinearity (1.201 in air)
$b(f_1, f_2)$	= bicoherence
c_0	= speed of sound
D_j	= jet nozzle diameter
$E[]$	= expectation operator
f	= frequency
$FT\{ \}$	= Fourier transform operator
$\text{Im}[]$	= Imaginary part
k	= acoustic wavenumber

¹ Assistant Professor, Dept. of Physics and Astronomy, N319 ESC, Provo UT, 84602, kentgee@byu.edu, AIAA Member

² Graduate Student, Dept. of Physics and Astronomy, N201 ESC, Provo UT, 84602.

³ Graduate Student, Grad. Prog. in Acoustics, 202 Applied Science Bldg., University Park PA, 16802, AIAA Student Member

⁴ Professor and Head, Grad. Prog. in Acoustics, PO Box 30, State College, PA, 16804, AIAA Member

⁵ Assistant Professor, REEF, 1350 N. Poquito Rd, Shalimar, FL 32579, AIAA Senior Member.

⁶ Senior Research Engineer, NCPA, Coliseum Dr., University MS, 38677, AIAA Senior Member.

⁷ Associate Director, NCPA, Coliseum Dr., University MS, 38677, AIAA Associate Fellow.

OASPL	=	overall sound pressure level
ρ_0	=	ambient density of air
$p(t)$	=	time-dependent acoustic pressure
p_{rms}	=	root mean-square pressure
$P(f)$	=	Fourier pressure spectrum
$Q_{p^2 p}(f)$	=	imaginary part of the cross-spectral density between $p^2(t)$ and $p(t)$, see Eq. (1)
r	=	range variable
$S_{pp}(r, f)$	=	power spectral density
$S_{ppp}(f_1, f_2)$	=	bispectral density, see Eq. (5)
T	=	time record length
$Z(f_1, f_2)$	=	bifrequency spectral density, see Eq. (6)
*	=	complex conjugation operator

I. Introduction

NONLINEARITY in the propagation of high-amplitude jet noise is a research topic that has been studied for decades. The combined results of early investigations such as those by Blackstock,¹ Morfey and Howell,² Crighton and Bashforth,³ Crighton,⁴ Lighthill,⁵ and Gallagher and McLaughlin⁶ showed that nonlinearity should be a factor in the noise propagation for certain conditions. However, much was left undone regarding the relative significance of these effects. Recently, there has been a renewal of interest in nonlinear jet noise propagation that is largely attributable to next-generation military jet fighters coming online. Petitjean and McLaughlin⁷ and Petitjean *et al.*⁸ have performed model-scale propagation experiments in anechoic facilities. From the full-scale jet perspective, Gee *et al.*^{9,10} have analyzed F/A-18E Super Hornet data for evidence of nonlinearity. Further indication of nonlinearity in full-scale jet noise propagation has come from work by Gee *et al.*¹¹ that involved field measurements of the noise radiated by the F-22 Raptor. Results from a nonlinear propagation model predicted significant waveform steepening and a spectral energy transfer to high frequencies that agreed closely with measured data.

Although the recent measurements have confirmed what has been suspected for decades regarding the nonlinear propagation of high-amplitude jet noise, both full-scale and model-scale experiments suffer from limitations. Measurements made to date have primarily shown evidence of nonlinear propagation by making a measurement at close range (but presumably in the geometric far field) and then assuming spherically spreading, free-field linear propagation out to a greater distance where this linear prediction is compared to measurement. For full-scale static measurements, this approach is potentially compromised by local meteorological effects (e.g., turbulence and refraction) and by terrain effects. Model-scale measurements are typically carried out in an anechoic laboratory environment but are limited by bandwidth and/or propagation distance considerations. In a spectral sense, the first evidences of nonlinear propagation are seen at high frequencies due to the nonlinear steepening of the time waveform. If the measurement bandwidth (transducer or data acquisition system) is insufficient, these effects will not be readily seen in power spectral comparisons unless the propagation distance is large enough. However, since the size of an anechoic facility imposes a constraint on the allowable propagation distance, limited propagation distance for a given measurement bandwidth is a further limitation. In an effort to maximize the comparison range, measurements that are assumed to be in the far field may be actually located in the geometric near field. This practice would cause comparisons between spectra using a simple linear model that assumes far-field propagation erroneous.

The primary purpose of this paper is to describe the use of alternative methods to show evidence of nonlinear propagation, particularly in model-scale measurements that might be limited by bandwidth or propagation distances. These methods, dubbed “nonlinearity indicators,” consist of bispectral and quadspectral analyses. After a summary of their underlying theories, these methods are applied to high-amplitude jet noise data collected at the National Center for Physical Acoustics in July 2005. The analysis is used to separate geometric near-field effects from nonlinear propagation effects. The investigation also results in some tentative conclusions regarding the onset of the geometric far field for supersonic jet noise.

II. Nonlinearity Indicators

Because research regarding nonlinearity indicators for acoustic propagation is relatively new and the limitations of various types are still being explored, two different indicators have been selected for use in this research: the normalized quadspectral density between the square of the acoustic pressure and the acoustic pressure (first looked at by Morfey and Howell²), and the bicoherence. The underlying theory and the potential utility of each of these two indicators are summarized in turn.

A. Quadspectral Analysis

In spectral analysis, the quadspectral density is defined as the imaginary part of the cross spectral density between two signals. The particular quantity that is useful as an indicator of nonlinear propagation is the quadspectral density between the square of the acoustic pressure and the acoustic pressure, namely

$$Q_{p^2p}(f) = \text{Im} \left[FT \{ p^2(t) \} FT^* \{ p(t) \} \right]. \quad (1)$$

Morfey and Howell² first recognized the potential of Q_{p^2p} as a nonlinearity indicator when they derived an ensemble-averaged version of the generalized Burgers equation (GBE), which may be written as

$$\frac{\partial}{\partial r} \left[r^2 e^{2\alpha(f)r} S_{pp}(r, f) \right] = -2\pi f r^2 \frac{\beta}{\rho_0 c_0^3} e^{2\alpha(f)r} Q_{p^2p}(r, f). \quad (2)$$

The GBE is a parabolic propagation equation that can incorporate nonlinearity, geometric spreading, and atmospheric absorption and dispersion. In Eq. (2), for which spherical spreading is assumed, the left-hand side represents the spatial rate of change of the power spectral density, $S_{pp}(r, f)$, that has been corrected for linear losses, namely spherical spreading (r^2) and atmospheric absorption ($e^{2\alpha(f)r}$). If an assumption of spherical spreading holds, then in the absence of nonlinearity, then Eq. (2) will be equal to zero, meaning that a power spectral density that is corrected for the linear losses it experiences during propagation will remain unchanged. Therefore, the right-hand side of Eq. (2) represents a quadratic source term that accounts for the sum/difference frequency generation that occurs during nonlinear propagation. At frequencies where the right-hand side is negative, there is a net energy loss due to nonlinearity (i.e., energy is being transferred to other frequencies). At frequencies where the right-hand side is positive, the energy net gain is positive.

Different forms of nonlinearity indicators have evolved from the right-hand side of Eq. (2). The first indicator, which has been used in analyses of jet and rocket noise data,^{2,9,12,13} is a dimensionless form that Morfey and Howell called Q/S that is written as

$$Q/S = \frac{Q_{p^2p}(f)}{S_{pp}(f) p_{rms}}. \quad (3)$$

A second indicator is the right-hand side of Equation (2) itself, which requires knowledge of both r and α . This indicator has been used^{8,13,14} because its results are more readily interpretable than Q/S . Physically, the right-hand side of Eq. (2) is the spatial rate of change of the power spectral density (PSD) due to nonlinearity as a function of frequency and range. The final form of this indicator, developed by Falco *et al.*,¹⁵ involves a summation of the right-hand side of Eq. (2) over frequencies where it is negative. A potential advantage of this approach is that it can be used more readily in situations where the measurement is significantly bandlimited.

There are potential limitations in the application of Morfey-Howell-based nonlinearity indicators to jet noise. First of all, the GBE fundamentally assumes the wave has reached the acoustical far-field, where $kr \gg 1$. This would limit low-frequency applicability for a given range, especially near the jet. Next, the GBE is most readily applied in situations where the type of geometric spreading is well-defined (e.g., sonic boom propagation, where the spreading is cylindrical.) Near a jet, the type of geometric spreading is very likely frequency-dependent and it is not until the range is much greater than the aeroacoustic source length that the spreading will be approximately spherical. Another limitation that arises in outdoor measurement situations is the fact that the GBE does not incorporate all relevant propagation phenomena. Environmental effects (e.g., wind, turbulence, ground) not

modeled by the GBE would effectively impact the right-hand side of Eq. (2) and could result in erroneous conclusions regarding the nonlinearity of the propagation. The final limitation, which has influenced studies that used the full right-hand side of Eq. (2), involves the dimensions of the equation. If the range, r , is assumed to be in meters, then the rate of nonlinear energy transfer for a model-scale jet and a full-scale jet with the same operating conditions could differ by orders of magnitude. If r is part of the nonlinearity indicator used, then the propagation distance should be normalized by the jet nozzle diameter (D_j). That is the approach taken in this study.

Despite the potential limitations of using a GBE-based nonlinearity indicator, there are also advantages that merit discussion as well. First of all, the GBE is a widely used model equation within the nonlinear acoustics community and very accurately describes parabolic propagation as long as its governing assumptions are met. Second, with a relatively simple calculation and frequency-domain plot, one can make judgments regarding which frequencies are losing and gaining energy due to nonlinearity. It should be noted that this is true regardless of the type of spreading, which simply constitutes a scaling factor in the right-hand side of Eq. (2). For that reason, provided that the acoustic far-field assumption is met, a GBE-based indicator is at least a *qualitative* indicator of nonlinearity. It can, therefore, be extremely useful in the present investigation, which is to distinguish nonlinear effects from geometric near-field effects in a laboratory jet noise measurement environment.

B. Bicoherence Analysis

The second type of nonlinearity indicator used in this analysis is the bicoherence, a dimensionless form of the bispectral density. The bicoherence is a quantity used in higher-order spectral analysis to identify quadratic nonlinearities in a signal. Quadratic nonlinearities reveal themselves in a propagating time waveform through sum- and difference-frequency generation, which causes the energy present at different frequencies to become phase coupled. This process is known as quadratic phase coupling (QPC). The bicoherence, first proposed by Kim and Powers,¹⁶ may be expressed as

$$b(f_1, f_2) = \frac{|S_{ppp}(f_1, f_2)|}{\sqrt{Z(f_1, f_2)S_{pp}(f_1 + f_2)}}. \quad (4)$$

In Eq. (4), the bispectral density is defined as

$$S_{ppp}(f_1, f_2) = \lim_{T \rightarrow \infty} \frac{1}{T} E[P(f_1)P(f_2)P^*(f_1 + f_2)] \quad (5)$$

and the bifrequency spectral density, $Z(f_1, f_2)$, is defined as

$$Z(f_1, f_2) = \lim_{T \rightarrow \infty} \frac{1}{T} E\left[|P(f_1)P^*(f_2)|^2\right]. \quad (6)$$

A more extensive discussion of bispectral theory, particularly digital bispectral estimation, may be found in Ref. 10 and additional references therein.

The bicoherence removes the dependence of $S_{ppp}(f_1, f_2)$ on signal power at a given frequency and provides a measure of the degree to which QPC exists among spectral components in a signal. However, $b(f_1, f_2)$ currently has a strict quantitative interpretation only if the signal is periodic. For a periodic signal with spectral components at f_1, f_2 , and $f_1 + f_2$, calculation of $b(f_1, f_2)$ yields the fraction of power at $f_1 + f_2$ that is present due to QPC between f_1 and f_2 .¹⁶ If the component at $f_1 + f_2$ exists solely because of a nonlinear interaction between f_1 and f_2 , then $b(f_1, f_2) \rightarrow 1$. However, for a nonlinear random noise signal, multiple bifrequencies may interact nonlinearly to yield a single component of $S_{pp}(f)$. Consequently, there is a cascading of sum and difference frequency generation that makes quantitative analysis of a bicoherence spectrum difficult. Greb and Rusbridge¹⁷ have investigated broadband spectral interactions in nonlinear plasma physics and have found that the maximum value of $b(f_1, f_2)$ may be reduced in an ill-defined manner which depends on both spectral shape and resolution. They suggest that

although the bicoherence is only useful for rather coarse spectral resolution, it is nevertheless helpful because its normalization allows the identification of nonlinear coupling that is undetectable without normalizing $S_{ppp}(f_1, f_2)$.

As with the GBE-based indicators, the bicoherence has benefits but also limitations. The principal benefit of bispectral analysis is that it does not depend explicitly on second-order wave equation assumptions and so can be used in both the acoustic and geometric near and far fields. Also, the use of bispectral analysis is widespread; it has been used to identify quadratic nonlinearities in data sets from fields ranging from economics to astronomy. The first limitation of bicoherence analysis has already been discussed, in that for a broadband jet noise signal, the strict quantifying of QPC is ill-defined. The other disadvantage of the bicoherence is that it seems to only detect the relative level of QPC in a signal, but does not independently indicate a direction of energy transfer. There is a higher-order spectral analysis technique known as cross-bispectral analysis; however, use of that quantity was not immediately more helpful than the bicoherence and needs further investigation.

There is another normalization of $S_{ppp}(f_1, f_2)$ that merits mention before the experiments and results are discussed. Hinich and Wolinsky¹⁸ have criticized the Kim and Powers¹⁶ normalization of $S_{ppp}(f_1, f_2)$ by demonstrating that $Z(f_1, f_2)$ can be shown to depend upon both the spectral resolution and upon the next higher-order spectrum, the trispectral density. They instead promote the use of a different normalization, originally formulated by Haubrich¹⁹ and later termed the skewness function.²⁰ Unlike the bicoherence, there is no upper bound on the skewness function. However, its variance is flat as a function of bifrequency, which allows signal linearity to be readily determined via a statistical test based on a chi-square distribution assumption. Although only $b(f_1, f_2)$ results are presented in this paper, the skewness function was also calculated and yielded very similar results. Therefore, in this application of bispectral analysis to identify nonlinearity in high-amplitude jet noise, the bicoherence normalization is likely sufficient, because conclusions are currently based on relative comparisons between measurement range, angle, and jet Mach number.

III. Experiment Description

A. Facility Description

An extensive set of model-scale jet noise data was collected at the National Center for Physical Acoustics in July 2005. The chamber has working dimensions of 5.8 m x 6.1 m x 2.4 m (18 ft x 19 ft x 8 ft) and is anechoic above 200 Hz. Although the facility is usually capable of producing highly heated jets, only unheated jets were used for the experiments reported here. Two different 3.49-cm (1.375-in) diameter round nozzles were used in the experiments described here, a Mach-0.85 (subsonic) nozzle and a Mach-2.0 (supersonic) nozzle. This yields a maximum scaled propagation distance of 80 jet diameters (D_j).

B. Data Collection and Processing

Acoustic pressure data were collected using a stepper-motor-controlled microphone boom that was designed and constructed at Penn State. Mounted on the boom, which is shown in Fig. 1, was a linear array of Bruel and Kjaer condenser microphones located at 10, 20, 30, 40, 60, and 75 D_j from the origin of the array. Based on Schleiren visualization of the jet noise field, the boom was set up such that its axis was located 4 D_j downstream of the nozzle exit plane in an attempt to locate the boom at the source of the Mach wave radiation in the supersonic jet noise case. The boom was rotated in 5° increments to obtain a finely sampled jet noise field from 80°-150°, where the angles are relative to the forward direction (see Fig. 2). In addition to the microphone boom, stationary Bruel and Kjaer 4939 microphones at 80 D_j were located at 150° and 90°. For each angle, 2²⁰ samples of time waveform data (about 5.5 s) were acquired with an eight-channel, 24-bit Motu Model 896 recorder with a sampling frequency of 192 kHz.

The boom microphones located at 10, 20, 40, and 60 D_j were 6.35-mm (0.25 in) diameter Bruel and Kjaer type 4938 microphones, whereas the 30 and 75- D_j microphones were 3.18-mm (0.125 in) type 4138 microphones. In order to provide the flattest response of these pressure-type microphones, they were mounted vertically on the boom at grazing incidence to the acoustic field. However, it was determined that response of the 6.35-mm microphones began to roll off at about 35 kHz, whereas the response of the 3.18-mm microphones appeared to be flat out to the maximum analysis frequency of 75 kHz. Consequently, at frequencies greater than 35 kHz, an amplitude correction was applied to the 6.35-mm B&K 4938 microphone data. The correction at 75 kHz was approximately 7 dB.

IV. Measurement and Linear Extrapolation Results

Spectral results for Mach 0.85 and Mach 2.0, calculated from the measured time waveform data, are presented in this section. Because of the large amount of data collected, only a subset of data is shown and discussed. In addition, a linear extrapolation analysis of the spectra is performed. This extrapolation, which consists of the application of spherical spreading and atmospheric absorption out to the greatest measurement distance, may be written for generic distances r_0 and r as

$$S_{pp}(r, f) = \frac{r_0^2}{r^2} e^{-2\alpha(f)[r-r_0]} S_{pp}(r_0, f). \quad (7)$$

In addition to linearity, this approach also inherently assumes that the data at r_0 were collected in the geometric far field. In Sec. V, deviations from linear, far-field behavior are further analyzed and separated into geometric near-field and nonlinear propagation effects.

A. Mach 0.85

For the Mach-0.85 jet, the measured PSDs at 90° are displayed in Fig. 3a. The results reveal the presence of geometric spreading manifested by the overall intensity decay as a function of distance. In addition, the spectral roll-off at high frequencies that increases as a function of distance shows the effects of atmospheric absorption on the noise propagation.

An important part of the analysis of the Mach-0.85 data involves a linear extrapolation of the 10–60- D_j data out to 75 D_j . The primary purpose of this extrapolation, which amounts to assumed free-field linear propagation between the measurement and extrapolation distances, is to use the PSD estimates at several distances to gauge the linearity of the propagation. As discussed before, this involves the application of spherical spreading and atmospheric absorption between the measurement distance and the extrapolation distance. It is worth noting that this approach is somewhat different than that often taken in jet noise data analyses. In a typical study, authors scale spectra to a reference distance near the source and attempt to remove the effects of atmospheric absorption to create a “lossless” spectrum. The intent is to be able to readily compare noise spectra that have been measured under different atmospheric conditions. Although the method is wholly accurate for far-field spectra and linear propagation, it may be ill-suited for high-amplitude (i.e., nonlinear) jet noise data analysis, especially over large extrapolation distances. The nonlinear propagation results in an energy transfer to high frequencies, which can mitigate the high-frequency spectral roll-off normally associated with atmospheric absorption. In fact, it was early measurements of aircraft noise where “anomalously low” atmospheric absorption was observed that caused researchers to suspect nonlinear propagation (e.g., see Ref. 2 and references therein). From a system input and output perspective, application of a linear transfer function to the spectrum when the system is nonlinear will yield nonphysical results. This nonphysical result is manifest by a “turn-up” at high frequencies in the “lossless” spectrum.

In Fig. 3b, the Mach-0.85 spectra at 10-60 D_j displayed previously in Fig. 3a have been linearly extrapolated out to 75 D_j using Eq. (7). The general collapse of the 10-60- D_j data (+/- 1 dB) suggests that the propagation is linear and that the source is aeroacoustically compact. A comparison of Figs. 3a and 3b reveals, however, that the 75- D_j PSDs exhibit some 1-2-dB spikes below 10 kHz. Because a) similar spikes are manifest in virtually every 75- D_j measurement, and b) a check of the data acquisition system itself with a nonacoustical input revealed no spikes, the cause of the spikes is likely reflections from boom surfaces that were not entirely wrapped with absorptive material. With the exception of the spikes, however, the 75- D_j measured PSD collapses with the extrapolated spectra, especially above 10 kHz.

These linear extrapolation results for the subsonic case merit further discussion regarding the definition and location of the geometric far field for subsonic jet noise. As mentioned previously, the measurement array was centered 4 D_j downstream from the nozzle exit plane. This was an attempt to collocate the measurement array with the dominant aeroacoustic source region for these particular experiments. The geometric far field in this context is understood to be where the intensity decay begins to look spherical along a given radial, which indicates a compact source. However, many researchers in the jet noise community define the geometric far field to be the location where an assumption that the noise originates as a spherically spreading source at the nozzle exhaust results in negligible error. Koch *et al.*²¹ and Viswanathan²² have recently published papers in which experimental results have been used to establish the location of the geometric far field (for the latter definition) for unheated round jets. In the Koch *et al.* experiments, Mach-0.5 and Mach-0.9 unheated jets were studied. In Viswanathan’s paper, the conditions investigated were Mach 0.6, 0.8, and 1.0. Koch *et al.* concluded that, for their definition of the geometric

far field, a spherically spreading compact source could only be assumed for distances greater than 50 jet diameters. They did note that high frequencies reached the far field as close as 8 diameters, but concluded that the extended nature of the low-frequency aeroacoustic sources pushed the overall far field to a greater distance. From his studies, Viswanathan found that the geometric far field began at about 35 jet diameters but his conclusions were made for “jet noise” in general without regard for jet source conditions (e.g., Mach number, temperature ratio, etc.).

The results from the current experiment suggest that for a subsonic jet, the noise source can be considered nearly aeroacoustically compact even at very close ranges. This conclusion is based on the collapse of the curves in Fig. 3b. However, if the acoustic array is centered at the nozzle exit plane, one has two effects to separate: a) when is the spreading spherical, and b) when can it be assumed that the noise originates at the nozzle? To demonstrate this principle, the experimental setup shown in Fig. 2 was modified in that the boom axis was moved to the nozzle exit plane. The linearly extrapolated spectra for 90° out to $75 D_j$ are displayed in Fig. 4. If the results in Fig. 4 are isolated and used by themselves, one could potentially conclude that the spreading from this subsonic jet is appreciably nonspherical at low frequencies. However, comparison with Fig. 3b, which showed essentially spherical spreading for the same jet, demonstrates that the failure of the extrapolations to collapse in Fig. 4 is caused by misalignment of the acoustic source with the measurement array axis. In other words, the spreading appears to be spherical but the noise source does not originate at the nozzle exit plane; to assume so can introduce significant errors into simple analyses. Finally, it is noted that the results in Fig. 4 do appear to corroborate the findings of Viswanathan for a subsonic jet in that the collapse of spectra measured beyond $30 D_j$ is ± 1 dB.

B. Mach 2.0

The limited set of Mach-0.85 results have been shown to describe the propagation of noise from a subsonic jet. In the nonlinearity indicator analysis section, these results will be used as a benchmark to demonstrate the behavior of the indicators for relatively low-amplitude noise signals. The measurement results for the supersonic Mach-2.0 jet, however, represent a significant increase in level from the subsonic jet. The OASPL as a function of both angle and radius is shown in a polar representation in Fig. 5. (For this and all subsequent measurements, the measurement array is centered at $4 D_j$ as shown in Fig. 2 rather than the nozzle exit plane.) The cause of the approximately 2-dB “bump” in the OASPL curves between 95° and 110° at all distances has not been determined; however, the data from those angles are not important to the subsequent analyses and are not considered further.

Unlike the previous Mach 0.85-case, a linear extrapolation analysis for the Mach-2.0 data reveals significant discrepancies between extrapolated and measured spectra. Three angles have been selected for analysis: 90° , 120° , and 145° , the last of which appears to correspond to the Mach wave angle for sufficiently large distances (see Fig. 5). The measured PSDs and corresponding linear extrapolations out to $75 D_j$, calculated according to Eq. (7), are shown in Figs. 6-8. In Fig. 6a, the 90° measured spectra show the effects of geometric spreading and atmospheric absorption, as there is an overall spectral decay but also increased losses at high frequencies as a function of range. Also apparent in Fig. 6a is a slight downward shift in peak frequency as a function of range. The linear extrapolation analysis in Fig. 6b demonstrates better collapse at high frequencies than at low, but does not collapse within ± 1 dB until beyond $40 D_j$. As was noted for the Mach-0.85 case, the spectral spikes below 10 kHz are present in the $75 D_j$ data, but the trend, especially above 10 kHz, follows those of the 40- and $60 D_j$ spectral densities.

In Fig. 7, the spectral and extrapolation results are presented for 120° . The OASPL at a given distance from the origin for this angle is approximately 5 dB greater than for the same distance and 90° . Figure 7a reveals similar behavior to that at 90° , in that there are the spectral decays due to geometric spreading and atmospheric absorption and a slight shift downward in peak frequency. In Fig. 7b, however, the general collapse of the extrapolated spectral densities at high frequencies is approximately 2 dB better than it was for 90° . At low frequencies, though, the collapse of the 120° data is slightly worse than the 90° data.

Figure 8 contains the measured and extrapolated spectral densities for 145° . These results represent a drastic change in behavior from the 90° and 120° data, beginning with an approximate 12 dB increase in OASPL from 120° . In Fig. 8a, there is a significant downward shift in peak frequency between $10 D_j$ - $60 D_j$. Between $60 D_j$ and $75 D_j$, there does not appear to be a downward shift, but this point is less definitive due to the spectral spikes at $75 D_j$. The other notable feature of the 145° PSDs in Fig. 8a that distinguish them from the behavior of the 90° and 120° data is the lack of apparent atmospheric absorption at high frequencies. The spectral slope beginning at about 20 kHz for $10 D_j$ is approximately the same for all subsequent measured spectral densities. The high-frequency roll-off that increases as a function of range (for linear propagation experiencing atmospheric absorption) is not present. The linear extrapolation analysis in Fig. 8b reinforces these points. An assumption of spherical spreading in the analysis provides a poor fit to the actual evolution of the PSD as a function of range. In fact, a comparison of the $10 D_j$ and

the 60- D_j reveals a 13 dB discrepancy between the two spectral densities at 3 kHz. In addition, the linear extrapolation analysis in Fig. 8b demonstrates what would happen to the approximate f^{-2} measured spectral slopes at high frequencies for ordinary linear propagation. Addition of absorptive losses, which appear to not show up in the measurement, as part of the linear extrapolation results in a steady increase in measured spectral levels at high frequencies relative to those linearly predicted as a function of propagation distance.

V. Nonlinearity Indicator Analysis

The Mach-2.0 jet noise results described in the previous section give rise to the key question of this investigation: Which of the behaviors shown in Figs. 6-8 that vary from far-field, linear propagation are related to near-field effects and which are caused by nonlinear propagation? Because of the supersonic, extended aeroacoustic source region for the Mach-2.0 jet, many of the boom measurements have likely been carried out in the geometric near field where an assumption of spherical spreading is invalid. (Note that placement of microphones in the geometric near field was intentional for the purposes of this study.) In addition, in the near field the propagation angles may not be well aligned with the measurement angles and so analyses of data acquired along a given radial may not be an accurate representation of the actual propagation. From a nonlinear standpoint, steepening of the time waveform will cause a transfer of energy from the peak-frequency region of the spectrum upward and possibly downward in the spectrum, which will cause an evolution of the spectrum that will differ from that predicted by linear theory. Consequently, there are potentially two causes for the results in Figs. 6-8: near-field effects and nonlinear propagation effects.

Examination of the measured and linearly extrapolated PSDs in Figs. 6-8 cannot conclusively separate near-field effects from nonlinear propagation effects because the PSD simply decomposes the spectral content present in the waveform as a function of frequency. There is no way of knowing the origin of the energy a given frequency band and whether it is quadratic-phase coupled to another band. For that reason, the spectrally based nonlinearity indicators described in Sec. II will be used to further analyze the propagation from these model-scale jets. Limited results from the Mach-0.85 jet are first presented to benchmark the behavior of the indicators for a linear propagation case. A more extensive analysis of the Mach-2.0 data is then carried out.

A. Mach 0.85

Provided that the measurement array was closely aligned with the dominant aeroacoustic source region for the subsonic jet, the linear, far-field propagation assumption applied via Eq. (7) resulted in little error (see Fig. 3b). The purpose of showing the Mach-0.85 nonlinearity indicator results is to characterize their behavior for a low-amplitude, linear propagation case. The first indicator shown is the quadspectral density-based indicator calculated from the right-hand side of Eq. (2), which represents the spatial rate of change of a linearly corrected PSD due to nonlinearity. As discussed in Sec. II, r is not expressed in meters, but rather in terms of the number of jet diameters, D_j . In Fig. 9, the calculated indicator is displayed for 90° and 60 D_j . The relatively low magnitude (compared with the Mach-2.0 results) and the fact that there are no distinct frequency regions separating positive and negative values suggests that nonlinearity is not a factor in the Mach-0.85 noise propagation. Figure 10 displays the bicoherence analysis results for the same microphone signal. For all frequencies, $b(f_1, f_2)$ is below the 99% confidence threshold for significant bicoherence, of which a conservative estimate is approximately 0.05.^{23,10} The results for $b(f_1, f_2)$ confirm that that QPC is negligible in the propagation of noise for the Mach-0.85 jet.

B. Mach 2.0

The previous subsection was instrumental in benchmarking the behavior expected of these nonlinearity indicators for low-amplitude noise propagation. For the Mach-2.0 data, where there are potentially both near-field and nonlinear effects, the nonlinearity indicators can be useful in separating the how these effects impact PSD evolution. For example, Figs. 6-8 each demonstrated deviation in measured spectra from expected far-field, linear propagation behavior. However, when the 90° and 120° data are analyzed using nonlinearity indicators, there is no evidence that the effects seen in Figs. 6b and 7b are due to nonlinear propagation effects. Displayed in Fig. 11 is the right-hand side of Eq. (2) calculated for various angles at 60 D_j . For 90°, 120°, and 130°, the indicator is very nearly zero (magnitudes are on the order of 10^{-3} to 10^{-2}) when compared to the 145° and 150° results, which are discussed subsequently. Figures 12 and 13 show $b(f_1, f_2)$ for 90° and 120° respectively, and although there are hints of significant bicoherence in Fig. 13, the QPC is generally negligible. These results indicate that the deviation from linear, far-field behavior in Figs. 6b and 7b is caused by near-field, not nonlinear effects.

At 145°, there were two spectral trends that disagreed with assumed far-field, linear propagation. First, Fig. 8b displayed a significant increase in spectral energy at low frequencies relative to the spherically extrapolated spectra, in addition to a downward shift in peak frequency. Second, there is an apparent lack of atmospheric absorption at high frequencies in the measured spectra (see Fig. 8a), which when compared against assumed linear propagation translates into greater measured energy at high frequencies than is linearly predicted (see Fig. 8b). The fundamental question is: Can either or both of these effects be explained in terms of nonlinear propagation?

As discussed before, Fig. 11 shows the Eq. (2)-based nonlinearity indicator at 60 D_j for various angles. Contrary to the lesser angles analyzed previously, 145° and 150° show clear trends in terms of nonlinear energy transfer. The curve for 145° shows that, from approximately 1.5-15 kHz, the net change in spectral energy due to nonlinearity is negative, meaning that these frequencies are losing energy. Above about 20 kHz, however, the indicator is clearly positive, which signifies that these frequencies are nonlinearly gaining energy.

Examination of the evolution of the quadspectral indicator as a function of range for fixed measurement angle is also helpful in studying the behavior of the noise propagation. In Fig. 14, the right-hand side of Eq. (2) has been calculated for each of the boom microphones along 145°. These curves each show a net flux of energy from the peak-frequency region of the PSD to higher frequencies. Although the downward shift in peak frequency present in Fig. 8 is tracked by the results in Fig. 14, note that there is no significant nonlinear energy transfer downward in the spectrum predicted by the indicator for any of the measurement distances. It is also noteworthy that the frequency region where the indicator switches from negative to positive values (12-20 kHz) is the same region in Fig. 8b above which greater spectral levels are measured than are linearly predicted.

The bicoherence analysis for the microphone measurements along 145° also reveals nonlinear propagation behavior, but in a different manner than the quadspectral density indicator. Displayed in Fig. 15 are $b(f_1, f_2)$ calculations for each of the six measurement distances. The comparison of the curves shows that the QPC in the signals increases as a function of range; therefore, $b(f_1, f_2)$ appears to be a cumulative indicator of the nonlinearity that has occurred to that point. Stated another way, the results in Fig. 15 indicate that the fraction of spectral energy at high frequencies that is caused by nonlinearity is increasing as a function of distance. Furthermore, Fig. 15 shows that the QPC generally occurs between the peak-frequency region of the spectrum and higher frequencies, which indicates an upward transfer of energy in the spectrum. The region of significant bicoherence shifts downward with the spectral peak in the PSD, but there is little indication of significant bicoherence at bifrequency pairs below the peak-frequency region. This result suggests that nonlinearity is primarily shifting energy upward in the spectrum and that the evolution of the spectrum in Fig. 8b around the peak-frequency region is not caused by nonlinear effects, but rather near-field directional and extended source effects. Consequently, it appears that shock coalescence, the nonlinear phenomenon that can result in a significant transfer of energy downward in the spectrum, is not a factor in the propagation of noise for the Mach-2.0 unheated jet.

One final point of discussion regarding these supersonic jet data regards the onset of the geometric far field for the Mach-2.0 unheated jet. The nonlinearity indicator analysis has revealed that the changes in the peak-frequency region of the spectrum relative to spherical spreading are primarily caused by geometric near-field effects. Examination of Figs. 6-8 in this context demonstrates that far-field, spherical spreading cannot be assumed for the Mach-2.0 unheated jet for distances closer than 60 D_j . The spectral spikes at 75 D_j preclude quantitative analysis of the onset of the far field beyond 60 D_j ; however, the similarity of the 60 and 75- D_j spectra suggest that the far field is at least being approached.

VI. Conclusion

The analysis in this paper has resulted in the primary conclusion that nonlinearity indicators, when coupled with ordinary spectral analysis, can be used to identify near-field and nonlinear effects in high-amplitude jet noise propagation. This technique is particularly applicable to high-amplitude noise measurements in model-scale jet facilities, where the maximum distances are usually fairly short. Future work in this area should include measurement made on supersonic, heated jets, because the OASPL for this case were relatively low (~137 dB re 20 μ Pa maximum at 10 D_j and 150°). Although this situation was sufficient to produce nonlinearity at high frequencies and peak directivity angles, jet conditions that produce significantly greater levels (more similar to military jet aircraft) should result in more significant nonlinear propagation effects. Such a study is required to better understand the potential role of acoustic shock coalescence on the evolution of the peak-frequency and low-frequency regions of the jet noise spectrum.

Additional research to be carried out involves developing a better quantitative understanding of these nonlinearity indicators. Although they are currently useful as a complement to power spectral analysis to better understand high-amplitude noise propagation, more work is needed to more fully understand the significance of

actual values of the quadspectral density-based and bicoherence indicators and how these they relate to the nonlinear evolution of a propagating jet noise waveform.

Acknowledgments

A portion of this work was supported by the Office of Naval Research.

References

- ¹Blackstock, D. T., "Nonlinear Propagation of Jet Noise," *Proceedings of the 3rd Interagency Symposium on University Research in Transportation Noise*, University of Utah, Salt Lake City, UT, 1975, pp. 389-397.
- ²Morfey, C. L., and Howell, G. P., "Nonlinear Propagation of Aircraft Noise in the Atmosphere," *AIAA Journal*, Vol. 19, No. 8, 1981, pp. 986-992.
- ³Crighton, D. G. and Bashforth, S., "Nonlinear Propagation of Broadband Jet Noise," AIAA paper no. AIAA-80-1039, June 1980.
- ⁴Crighton, D. G., "Nonlinear Acoustic Propagation of Broadband Noise," in *Recent Advances in Aeroacoustics*, edited by A. Krothapalli and C. A. Smith, Springer Verlag, New York, 1986, pp. 411-454.
- ⁵Lighthill, J., "The Inaugural Theodorsen Lecture: Some Aspects of the Aeroacoustics of High-Speed Jets", *Theoretical and Computational Fluid Dynamics*, Vol. 6, Nos. 5-6, 1994, 261-280.
- ⁶Gallagher, J. A. and McLaughlin, D. K., "Experiments on the Non-linear Characteristics of Noise Propagation from Low and Moderate Reynolds Number Supersonic Jets," AIAA paper no. AIAA-81-2041, Oct. 1981.
- ⁷Petitjean, B. P. and McLaughlin, D. K., "Experiments on the Nonlinear Propagation of Noise from Supersonic Jets," AIAA paper no. AIAA-2003-3127, May 2003.
- ⁸Petitjean, B. P., Viswanathan, K., and McLaughlin, D. K., "Acoustic Pressure Waveforms Measured in High Seed Jet Noise Experiencing Nonlinear Propagation," 43rd AIAA Aerospace Sciences Meeting and Exhibit, 2005, AIAA 2005-209.
- ⁹Gee, K. L., Gabrielson, T. B., Atchley, A. A., and Sparrow, V. W., "Preliminary Analysis of Nonlinearity in Military Jet Aircraft Noise Propagation, *AIAA Journal* Vol. 43, No. 6, 2005, pp. 1398-1401.
- ¹⁰Gee, K. L., Atchley, A. A., Falco, L. E., Gabrielson, T. B., and Sparrow, V. W., "Bispectral Analysis of High-amplitude Jet Noise," AIAA paper no. AIAA-2005-2937, May 2005.
- ¹¹Gee, K. L., Sparrow, V. W., James, M. M., Downing, J. M., Hobbs, C. M., Gabrielson, T. B., and Atchley, A. A., "Measurement and Prediction of Noise Propagation from a High-power Jet Aircraft," AIAA paper no. AIAA-2006-2531, May 2006.
- ¹²McInerny, S. A., and S. M. Ölçmen, "High-intensity Rocket Noise: Nonlinear Propagation, Atmospheric Absorption, and Characterization," *J. Acoust. Soc. Am.*, Vol. 117, No. 2, 2005, pp. 578-591.
- ¹³Gee, K. L., Petitjean, B. P., McLaughlin, D. K., and Sparrow, V. W., "Nonlinear Propagation of Noise Radiated from Supersonic Jets," *Proceedings of Noise-Con 04*, edited by C. B. Burroughs and G. C. Maling, Jr., Noise Control Foundation, Poughkeepsie, New York, 2004, pp. 725-733.
- ¹⁴Falco, L. E., Gee, K. L., Atchley, A. A., and Sparrow, V. W., "Investigation of a Single-Point Nonlinearity Indicator in One-Dimensional Propagation," Forum Acusticum Paper # 703, Budapest, Aug. 2005.
- ¹⁵Falco, L. E., Atchley, A. A., and Gee, K. L., "Investigation of a Single-Point Nonlinearity Indicator in the Propagation of High-Amplitude Jet Noise," AIAA paper no. AIAA-2006-2529, May 2006.
- ¹⁶Kim, Y. C. and Powers, E. J., "Digital Bispectral Analysis and its Applications to Nonlinear Wave Interactions," *IEEE Transactions on Plasma Science*, Vol. PS-7, No. 2, 1979, pp. 120-131.
- ¹⁷Greb, U. and Rusbridge, M. G., "The Interpretation of the Bispectrum and Bicoherence for Non-linear Interactions of Continuous Spectra," *Plasma Physics and Controlled Fusion*, Vol. 30, No. 5, pp. 537-549.
- ¹⁸Hinich, M. J. and Wolinsky, M., "Normalizing Bispectra," *Journal of Statistical Planning and Inference*, Vol. 130, 2005, pp. 405-411.
- ¹⁹Haubrich, R. A., "Earth Noise, 5 to 500 Millicycles per Second," *Journal of Geophysical Research*, Vol. 70, No. 6, 1965, pp. 1415-1427.
- ²⁰Hinich, M. J., "Testing for Gaussianity and Linearity of a Stationary Time Series," *Journal of Time Series Analysis*, Vol. 3, No. 3, 1982, pp. 169-176.
- ²¹Koch, L. D., Bridges, J., Brown, C., and Khavaran, A., "Experimental and Analytical Determination of the Geometric Far Field for Round Jets," *Noise Control Engineering Journal*, Vol. 53, No. 1, 2005, pp. 20-29.
- ²²Viswanathan, K., "Instrumentation Considerations for Accurate Jet Noise Measurements," *AIAA Journal*, Vol. 44, No. 6, 2006, pp. 1137-1149.
- ²³Elgar, S. and Guza, R. T., "Statistics of Bicoherence," *IEEE Transactions on Acoustics, Speech, and Signal Processing*, Vol. 36, No. 10, 1988, pp. 1667, 1668.



Figure 1. Photograph showing nozzle and microphone boom in the NCPA anechoic jet noise facility.

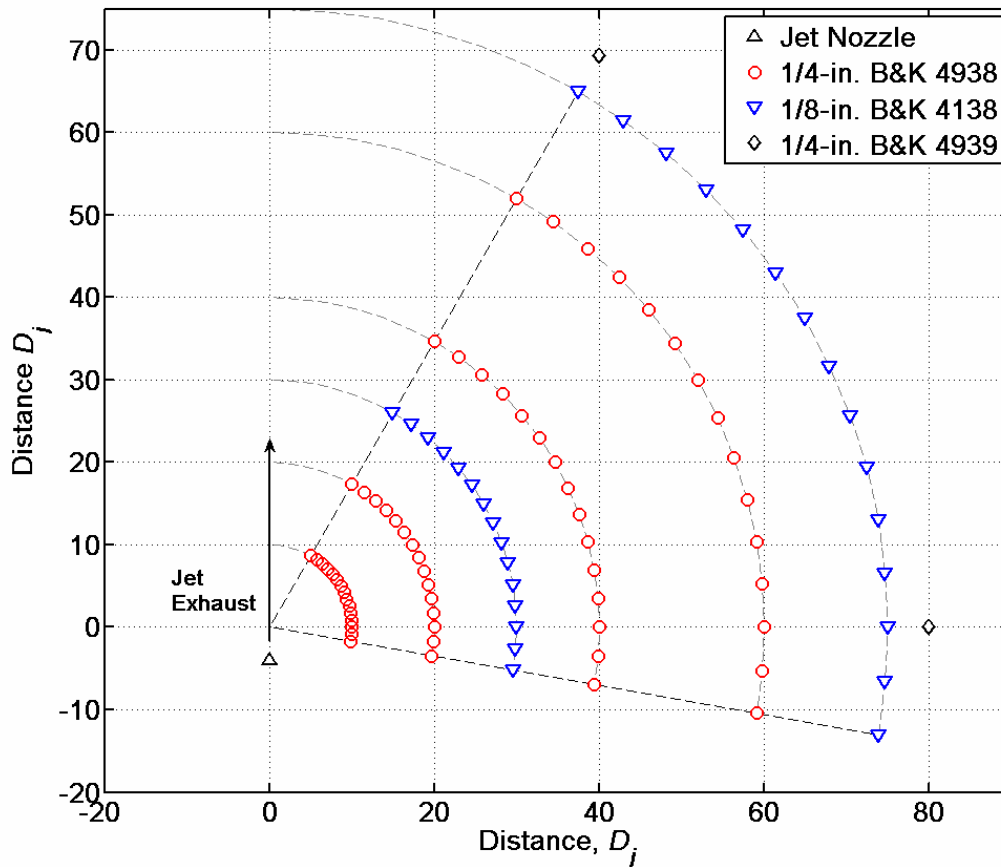


Figure 2. Diagram of microphone measurement locations, from 80°-150°, measured from the forward direction.

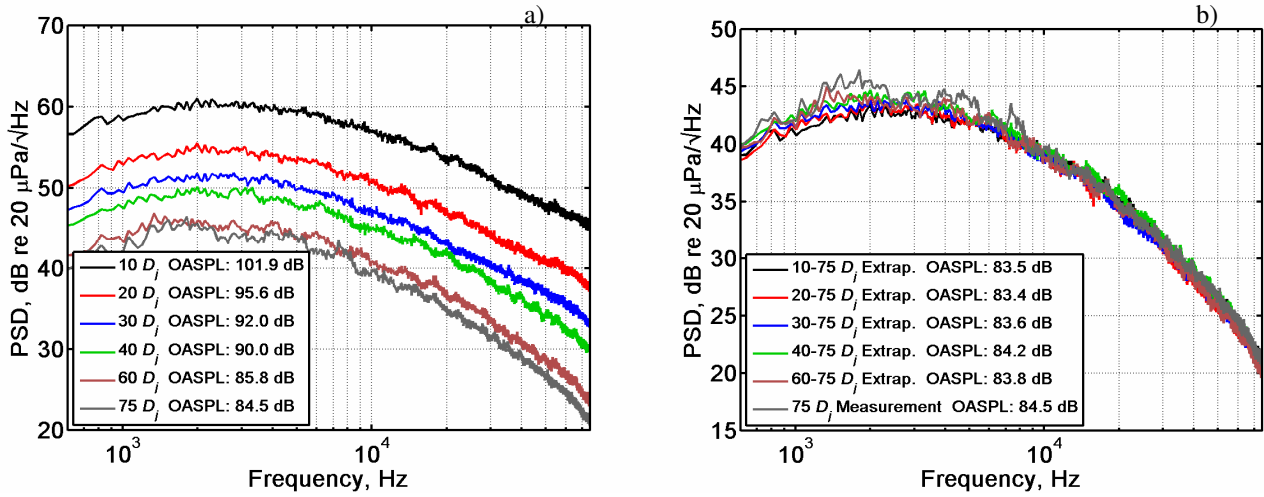


Figure 3. a) Measured power spectral densities for the Mach-0.85 jet at 90° , with the measurement array configured as shown in Fig. 2. b) Comparison of linearly extrapolated PSDs with the measurement at $75 D_j$.

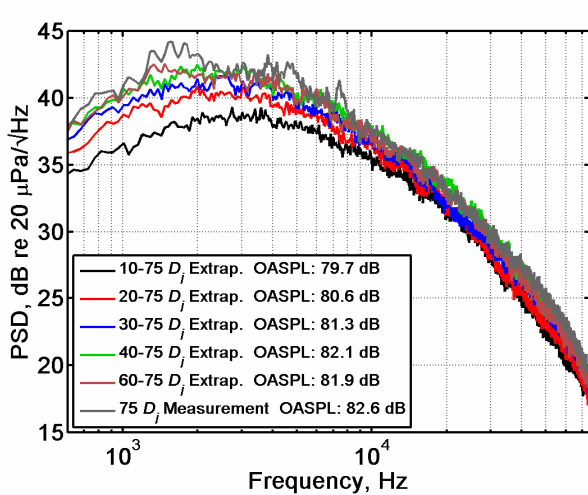


Figure 4. Linearly extrapolated PSDs out to $75 D_j$ for the Mach-0.85 jet at 90° , but with the measurement array centered at the nozzle exit plane rather than $4 D_j$ downstream.

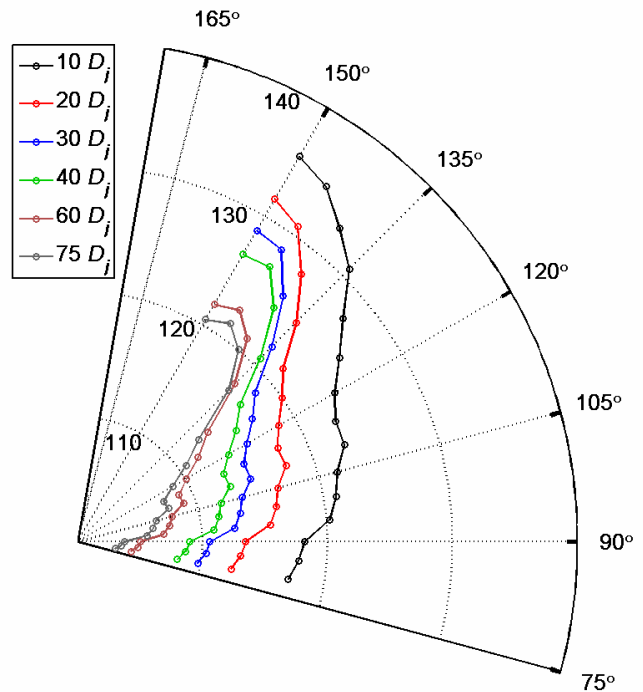


Figure 5. OASPL (in dB re $20 \mu\text{Pa}$) for the Mach 2.0 jet from 80° to 150° . The measurement array for all Mach-2.0 data was configured as shown in Fig. 2.

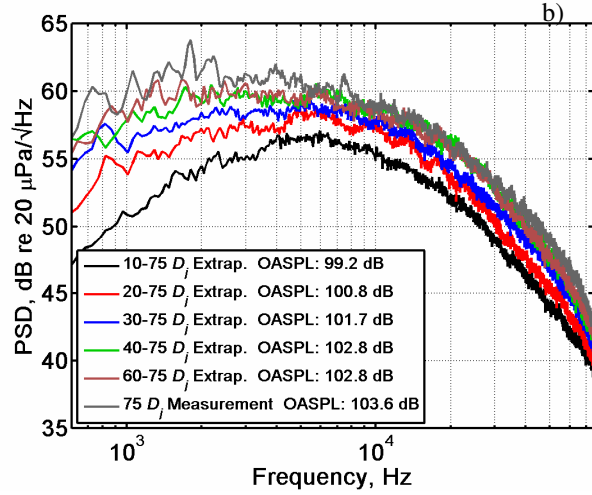
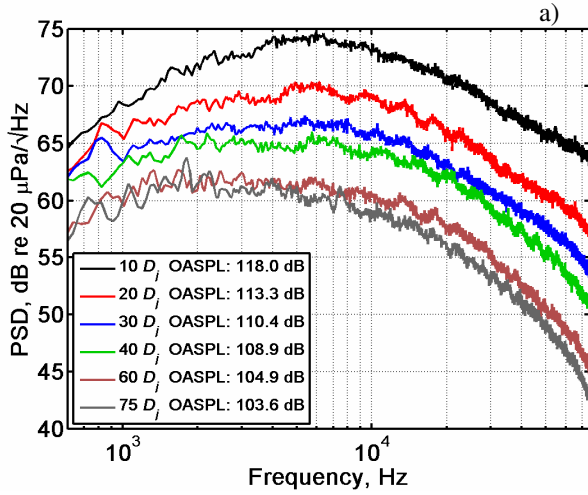


Figure 6. a) Power spectral densities for the Mach-2.0 jet at 90° . b) Comparison of linearly extrapolated PSDs at $75 D_j$ for 90° .

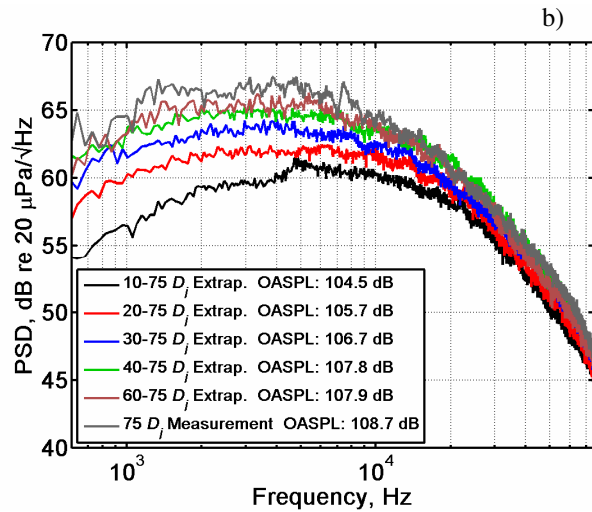
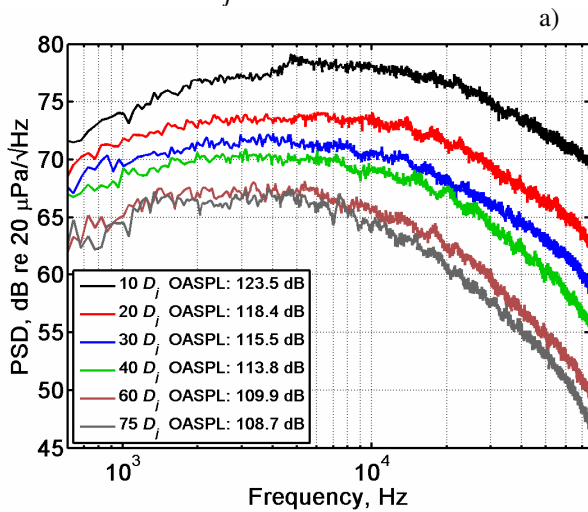


Figure 7. a) Power spectral densities for the Mach-2.0 jet at 120° . b) Comparison of linearly extrapolated PSDs at $75 D_j$ for 120° .

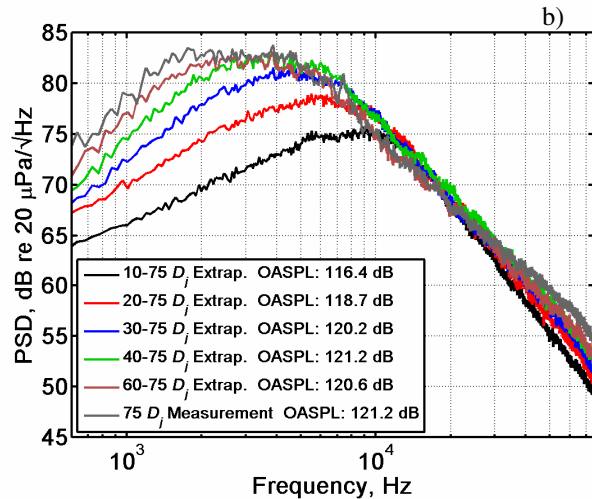
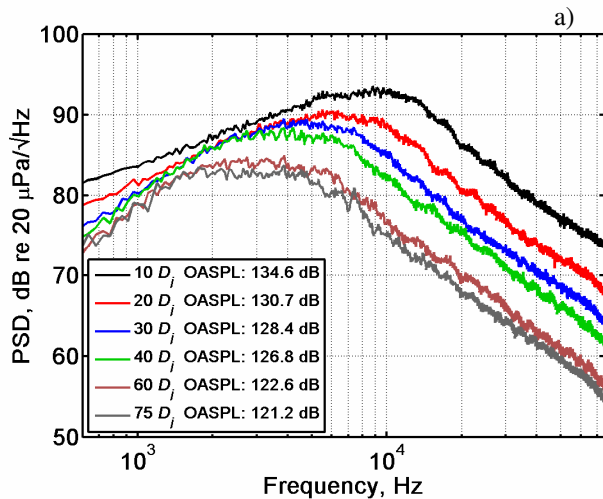


Figure 8. a) Power spectral densities for the Mach-2.0 jet at 145° . b) Comparison of linearly extrapolated PSDs at $75 D_j$ for 145° .

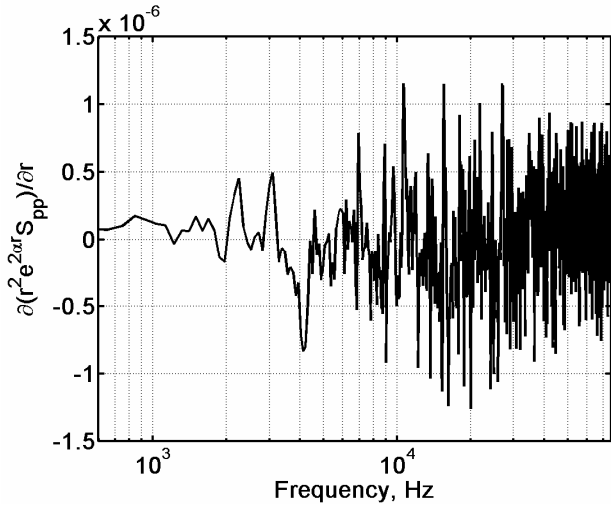


Figure 9. Nonlinearity indicator calculated from the right-hand side of Eq. (2) for the Mach-0.85 jet at 90° and $60 D_j$.

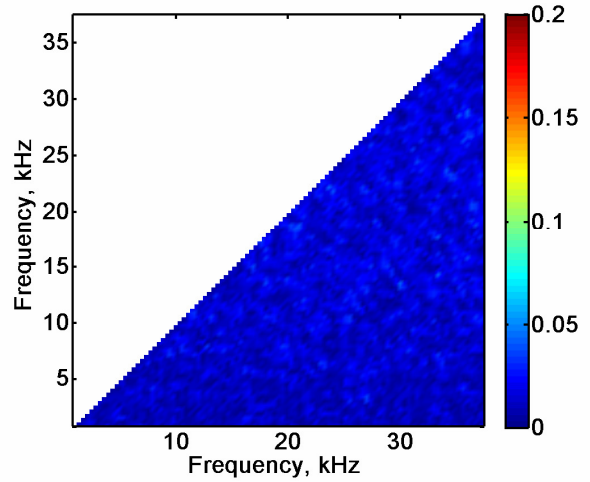


Figure 12. Bicoherence for the Mach-2.0 jet at 90° and $60 D_j$.

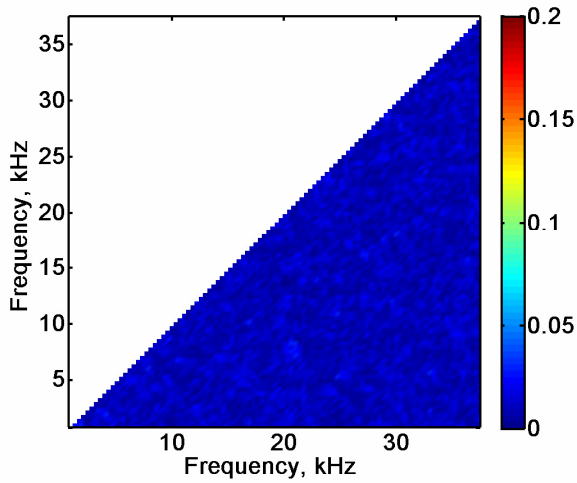


Figure 10. Bicoherence for the Mach-0.85 jet at 90° and $60 D_j$.

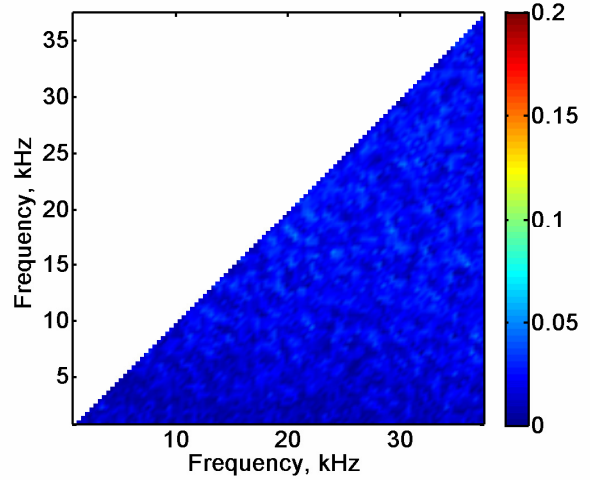


Figure 13. Bicoherence for the Mach-2.0 jet at 120° and $60 D_j$.

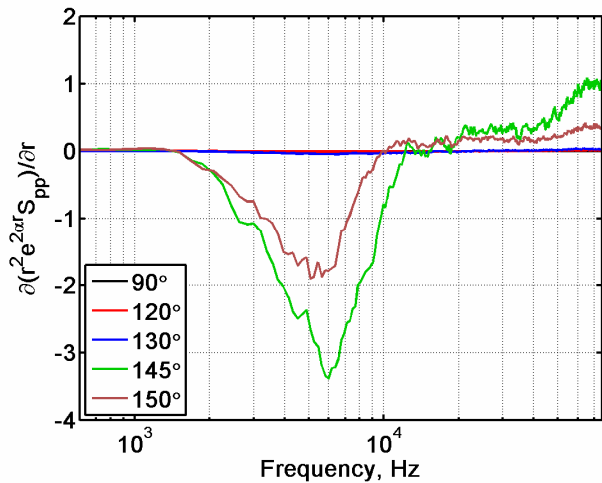


Figure 11. Equation (2)-based indicator for the Mach-2.0 jet at various angles and $60 D_j$.

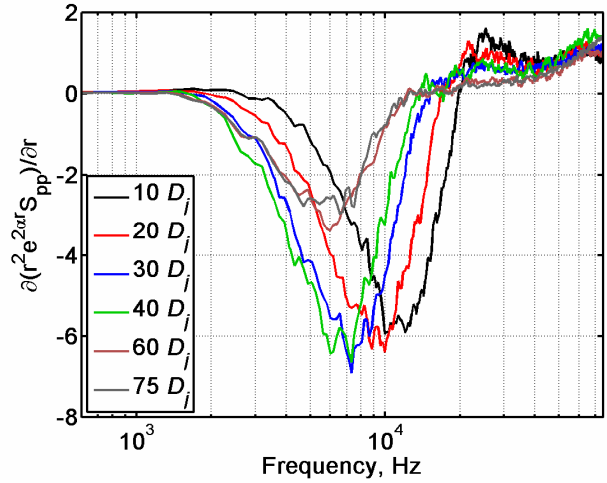


Figure 14. Equation (2)-based indicator calculated at the boom microphones for the Mach-2.0 jet at 145° .

Figure 15. Bicoherence for the Mach-2.0 jet at 145° for $10-75 D_j$, shown sequentially in Figs. a-f.

